Transp Porous Med (2012) 92:145–164
DOI 10.1007/s11242-011-9895-6

A Dynamic Network Model for Two-Phase Flow in Porous Media

Glenn Tørå · Pål-Eric Øren · Alex Hansen

Received: 22 January 2010 / Accepted: 8 October 2011 / Published online: 24 November 2011

Abstract We present a dynamic model of immiscible two-phase flow in a network representation of a porous medium. The model is based on the governing equations describing two-phase flow in porous media, and can handle both drainage, imbibition, and steady-state displacement. Dynamic wetting layers in corners of the pore space are incorporated, with focus on modeling resistivity measurements on saturated rocks at different capillary numbers. The flow simulations are performed on a realistic network of a sandpack which is perfectly water-wet. Our numerical results show saturation profiles for imbibition in agreement with experiments. For free spontaneous imbibition we find that the imbibition rate follows the Washburn relation, i.e., the water saturation increases proportionally to the square root of time. We also reproduce rate effects in the resistivity index for drainage and imbibition.

Keywords Network model · Two-phase flow · Reconstructed porous media · Imbibition · Resistivity index

1 Introduction

Petrophysical parameters like relative permeability, residual saturation and electrical resistivity are key parameters to predict the production of oil and gas from reservoirs. Traditionally such parameters are measured by laboratory testing on core plugs, which is a time-consuming process. Computer simulation of multiphase flow on a network has the advantage that it is far less time-consuming than doing experiments, or doing flow simulations on a grid

G. Tørå · A. Hansen (✉)
Department of Physics, Norwegian University of Science and Technology, 7491 Trondheim, Norway
e-mail: Alex.Hansen@ntnu.no

P.-E. Øren
Numerical Rocks AS, Stiklestadveien 1, 7041 Trondheim, Norway
e-mail: peoe@numericalrocks.com

model of the pore space. Another advantage over grid-based models (e.g. Lattice Boltzmann model) is that network models allow infinite geometrical resolution. This is an important feature in order to capture thin wetting layers residing in corners and crevices in the pores space. Wetting layers are stabilized by capillary forces, and have a significant effect on the resistivity of saturated rocks.

The networks are constructed by simplifying the pore-space into a network of interconnected pores and throats. Realistic networks have been introduced the last decades (Bryant and Blunt 1992). The networks may be extracted from a real pore space, which is generated from microtomographic images and process based reconstruction (Øren and Bakke 2003; Bakke and Øren 1997). In this way, the shape of each pore and throat is simplified, but the pore-size distribution and topology are preserved. The flow models are based on pore-scale displacements observed in micromodel experiments (Lenormand et al. 1983). By controlling parameters like pore-size disorder, viscosity, and flow rate, simulation of multiphase flow on networks has proved to be an attractive way of understanding the mechanisms of multiphase flow in porous media.

Among the first approaches to flow simulation on a network was the invasion percolation method, proposed by Wilkinson and Willemsen (1983) as a description of drainage in a porous medium. The premise for this method is the quasi-static flow condition that neglects the effects of viscous forces. The quasi-static model is at present the state of the art model to simulate multiphase flow at low capillary numbers. It has provided not only more insight in the physics of multiphase flow in porous media, but also the ability to predict petrophysical parameters (Øren et al. 1998; Bakke and Øren 1997; Valvatne and Blunt 2004; Patzek 2000; Man and Jing 2001).

However, in some cases the slow flow condition for the quasi-static model is not met, such as in highly permeable rocks, surfactant flooding, fractures, and in the vicinity of wells. In these cases, viscous forces can have significant effect on the fluid displacement, such as mobilization of discontinuous phases.

In order to capture the effects of viscous forces, the dynamic flow models have been developed (Dias and Payatakes 1986a,b; Lenormand et al. 1988; Aker et al. 1998; Hashemi et al. 1998; Dahle and Celia 1999; Hughes and Blunt 2000; Knudsen et al. 2002; Ferer et al. 2003). They take into account both the capillary and viscous pressure drops, and dynamic models are thereby not limited to low capillary numbers. The term "fully" dynamic is sometimes used when the capillary pressure is included in the pressure solver, and a small timestep is used.

In the last decade, there have been different approaches to include wetting layer flow into dynamic network models. For example, Mogensen and Stenby (1998) developed a fully dynamic model. To avoid solving a nonlinear equation for the pressures every timestep, they assumed a fixed thickness and conductance of the wetting layers. Another simulator of imbibition was reported by Constantinides and Payatakes (2000). They studied the effects of precursor wetting layers in primary imbibition. Microroughness was introduced, and the wetting layers advanced due to capillary suction of micromenisci. Singh and Mohanty (2003) studied the flow regimes in drainage with a dynamic model. They considered the bulk flow and layer flow as two linear flow problems. The two pressure solutions gave the capillary pressure and the layer thickness. The non-linearity of the problem was approximated by a heuristic approach. Nguyen et al. (2004) developed a realistic model for swelling of the wetting layers in imbibition. They assumed constant pressure in the nonwetting phase, and used a quasi-static approach for the frontal displacement. They modeled the swelling of wetting layers as a nonlinear diffusion process driven by the capillary pressure gradients, which is observed in capillary tubes by Dong and Chatzis (1995). The model is able to

reproduce the rate dependent competition between snap-off and frontal displacement in a realistic manner. However, the quasi-static approach limits the model to low capillary numbers. A fully dynamic model with wetting layer flow for both drainage and imbibition was developed by Al-Gharbi and Blunt (2005). Pressures were found solving a single phase problem, and fractional flow rates was calculated using equivalent hydraulic resistances. Wetting layer thickness given by capillary pressure at main menisci enabled a unique determination of fluid configuration in a pore/throat from known volume of wetting phase. They studied viscous effects on fractional flow curves. Recently, Idowu and Blunt (2009) developed a rule-based model for imbibition based on a model by Hughes and Blunt (2000), in which they extend the invasion percolation algorithm to include viscous pressure drops in both phases. Pressure drops across menisci are not included in the pressure solution, hence mobilization of trapped clusters is not possible. To reduce the computational cost, they allow several elements to fill every timestep. It makes this type of model much faster than fully dynamic models, where the pressure distribution is updated every timestep.

As far as we know, none of the existing network models incorporate dynamic wetting layers and viscous effects in both drainage, imbibition and steady-state. There has also been little focus on modeling resistivity measurements in dynamic network models. In this article, we present a dynamic model for two-phase flow in a network. It is an extension of the previous model proposed by Aker et al. (1998), and accounts for the dynamics of wetting layers. It is fully dynamic, and may be used as a unified model for both drainage, imbibition and steady-state. However, this can not be realized without a significant increase in computational cost, compared to more rule-based network models. As a validation of the model, we use it to study saturation profiles of imbibition. We also look at the resistivity index for drainage and imbibition at different capillary numbers, and the free spontaneous imbibition rate. The network we use in this study is reconstructed from a realistic pore space of a sandpack. Following this study, the model has been applied to steady-state simulations of electrical resistivity in sandstones (Tørå et al. 2010).

2 The Model

We base our model on the model proposed by Aker et al. (1998). In order to incorporate wetting layers in the model, the tubes have angular corners where the wetting fluid can flow between the nonwetting fluid and the tube walls. The cross-sectional shape is characterized by a dimensionless shape factor, G, defined as $G = A/P^2$ (Mason and Morrow 1991). A is the cross-sectional area, and P is the perimeter length. In this work, we use equilateral triangular shape of the cross-section of the tubes with $G = 0.048$ (see Fig. 1a). A characteristic feature of the model is that the nodes have no volume, so the tubes consist of both the pore and throat volume. A tube IJ is characterized by a length l_{IJ}, a throat radius r_{IJ} in the middle of the tube, and two pore radii r_{I} and r_{J} in the nodes connected to the tube (see Fig. 1b). The wetting fluid exists in all tubes, either as bulk or layer, giving the wetting fluid the same connectivity as the network itself. The throats and pores in a porous medium are represented by a network of tubes connected to each other through nodes, as shown in Fig. 2a. The electrical analog in Fig. 2b shows how the bulk flow and layer flow is separated in two parallel networks, connected where there are menisci. We assume a perfectly water-wet network with contact angle $\theta = 0$. Across a meniscus at position x in a tube, we assume a static capillary pressure

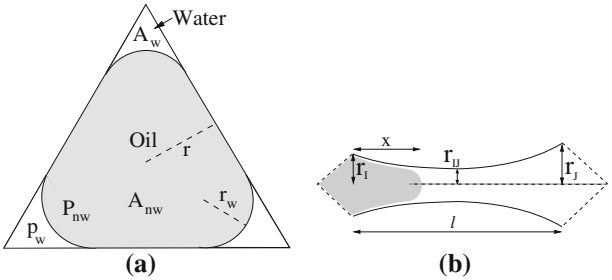

Fig. 1 **a** Crossection of a tube. r is the inscribed radius, r_{w} is the radius of curvature of the arc meniscus, A_{w} and A_{nw} are the cross-sectional areas of the wetting (water) and nonwetting phase (oil), respectively. P_{nw} is the nonwetting pressure, and p_{w} is the wetting pressure. **b** Illustration of one single tube

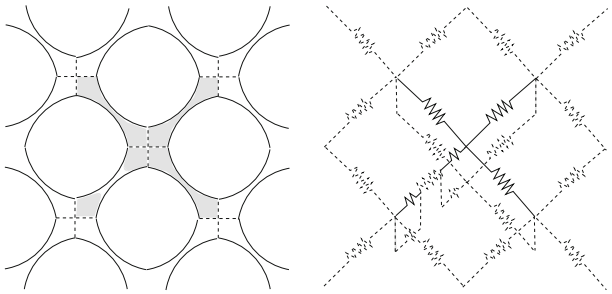

Fig. 2 **a** Illustration of how the tubes are connected to eachother through the nodes at the intersections of the *dashed lines*. Nonwetting fluid is *shaded*, and wetting fluid is *white*. **b** Electrical analog of the network. The bulk flow and layer flow is separated into an upper and lower network, respectively. The two networks are connected where there are menisci. Nonwetting fluid is drawn as *solid lines*, while wetting fluid is drawn as *dashed lines*

$$P_{\mathrm{c}}(x) = \gamma \frac{1 + 2\sqrt{\pi G}}{r(x)}, \tag{1}$$

where $r(x)$ is the inscribed radius, and γ is the interfacial tension. $P_{\mathrm{c}}(x)$ varies sinusoidally to give the tubes an effective shape of an hourglass.

2.1 Fluid Configurations

To simplify the movement of the fluids within a tube, only certain configurations are allowed. They consist of different fluid elements, and a conductance and flow rate are assigned to each element. The maximum number of menisci in each tube at the same time is restricted to two, and only the configurations shown in Fig. 3 are possible.

2.2 Computing the Hydraulic Conductances

By neglecting flow in thin films between the oil and solid, the cross-sectional areas open to flow are given by Bakke and Øren (1997)

$$A_{\mathrm{w}} = r_{\mathrm{w}}^2 \left(\frac{1}{4G} - \pi \right), \tag{2}$$

for the water layer, and

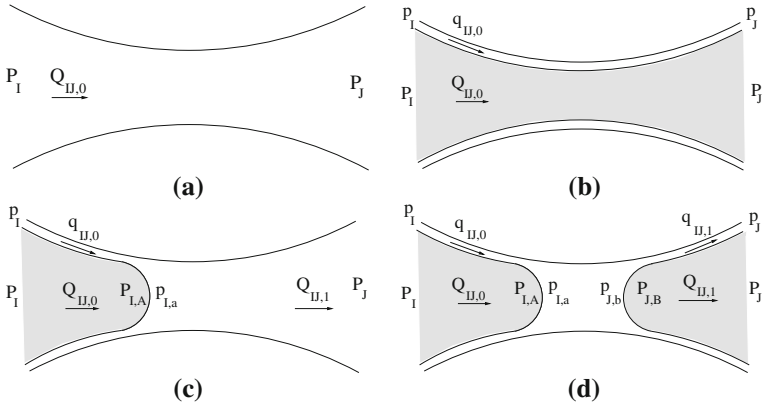

Fig. 3 The four configurations: **a** Only water present in tube. **b** Water present in layer and oil present in bulk. **c** Only one meniscus present in the tube (facing either direction). **d** Two menisci present with the water in the middle of the tube. $Q_{\mathrm{IJ},0}$ and $Q_{\mathrm{IJ},1}$ are the flow rates in the bulk, $q_{\mathrm{IJ},0}$ and $q_{\mathrm{IJ},1}$ are the flow rates in the water layer, P_{I} and P_{J} are the node pressures in the bulk, and p_{I} and p_{J} are the node pressures in the water layers

$$A_{\mathrm{nw}} = \frac{r^2}{4G} - A_{\mathrm{w}}, \tag{3}$$

for the oil. r_{w} is the radius of curvature for the arc meniscus, and r is the inscribed radius of the tube. By assuming that r_{w} is much smaller than the radius of curvature along the length of the tubes, the Young–Laplace equation yields

$$r_{\mathrm{w}} = \frac{\gamma}{P_{\mathrm{c}}}, \tag{4}$$

where P_{c} is the capillary pressure across arc menisci. The hydraulic conductance of a water layer element is given by Hagen–Poiseuille's law

$$g_{\mathrm{w}} = \frac{r_{\mathrm{w}}^2 A_{\mathrm{w}}}{8\beta\mu_{\mathrm{w}} l}, \tag{5}$$

where β is a flow resistance factor, μ_{w} is the water viscosity, and l is the length of the element. We use no-slip boundary condition giving $\beta = 5.3$ (Ransohoff and Radke 1988). For the bulk conductance, a mean hydraulic radius R is used, defined as

$$R_{\mathrm{i}} = \frac{1}{2}(r + r_{\mathrm{v,i}}), \quad \mathrm{i} = \mathrm{w}, \mathrm{nw}, \tag{6}$$

where $r_{\mathrm{v,i}}$ is an equivalent volume radius defined as

$$r_{\mathrm{v,i}} = \sqrt{\frac{A_{\mathrm{i}}}{\pi}}, \quad \mathrm{i} = \mathrm{w}, \mathrm{nw}. \tag{7}$$

The hydraulic conductance of a bulk element is given by

$$g_{\mathrm{i}} = \frac{R_{\mathrm{i}}^2 A_{\mathrm{i}}}{8\mu_{\mathrm{i}} l}, \quad \mathrm{i} = \mathrm{w}, \mathrm{nw}. \tag{8}$$

If fluid i is oil, then A_{i} is given by Eq. 3. If fluid i is water, then $A_i = A_{\mathrm{tot}} = r^2/4G$. For simplicity, the inscribed radius r can only take three values, r_{I}, r_{J} or r_{IJ}. Boundaries between pore and throat are defined at one third and two thirds of the tube length. The effective bulk

conductance of elements spanning pore/throat boundaries are given by the harmonic mean of the pore and throat conductances.

To calculate the water saturation S_w, a bulk water volume is given by

$$V_{\text{bulk}} = \int_{x_1}^{x_2} A_{\text{tot}}\, \mathrm{d}x, \tag{9}$$

where for simplicity, A_{tot} is assumed to vary linearly between the three fixed areas at r_I, r_J and r_{IJ}. The volume of a water layer element is given by $V_{\text{layer}} = A_w(x_2 - x_1)$.

2.3 Solving for Pressures

We define a pressure P in the bulk flow in the nodes, and p in the water layer in the nodes. We assume Poiseuille flow, hence, a linear relation between local flow rate of a fluid element and pressure drop across the element. As an example we set up the equations for configuration (D) in Fig. 3,

$$Q_{IJ,0} = g_{IJ,0}(P_I - P_{I,A}) \tag{10}$$
$$Q_{IJ,1} = g_{IJ,1}(P_{J,B} - P_J) \tag{11}$$
$$q_{IJ,0} = g_{IJ,2}(p_I - p_{I,a}) \tag{12}$$
$$q_{IJ,1} = g_{IJ,3}(p_{J,b} - p_J) \tag{13}$$
$$Q_{IJ,0} + q_{IJ,0} = Q_{IJ,1} + q_{IJ,1} = g_{IJ,4}(p_{I,a} - p_{J,b}), \tag{14}$$

where $g_{IJ,0}$ to $g_{IJ,4}$ are the hydraulic conductances in the respective fluid elements. The capillary pressure drops across the menisci are given by

$$P_{I,A} = p_{I,a} + P_c(IJ, x_1) \tag{15}$$
$$P_{J,B} = p_{J,b} + P_c(IJ, x_2), \tag{16}$$

where x_1 and x_2 are the positions of the menisci. From the above equations, we eliminate the pressures p_a, p_b, P_A, and P_B in the tube, and end up with the four flow rates as functions of the four unknown pressures in the nodes, P_I, p_I, P_J, and p_J. To solve for these pressures, we impose the condition that the net flux through a node of the bulk flow and the layer flow is zero. This gives a set of equations

$$\sum_J q_{IJ} = 0 \quad \sum_J Q_{IJ} = 0, \tag{17}$$

where J runs over the tubes connected to node I, and Q and q are flowrates into or out of node I. The equations can be written in the form

$$\mathbf{A}(\mathbf{p})\mathbf{p} = \mathbf{b}(\mathbf{p}), \tag{18}$$

where $\mathbf{p}$ includes the node pressures P and p. $\mathbf{A}(\mathbf{p})$ is a matrix of the conductances, and $\mathbf{b}(\mathbf{p})$ is a vector dependent on the outlet and inlet pressures, and the conductances of the tubes connected to the outlet and inlet. This is a system of nonlinear equations where the conductance of a tube is dependent on the pressures through Eq. 4. It can be solved with for example successive substitution (Mogensen et al. 1999), but is very computational expensive. However, assuming $\mathbf{A}(\mathbf{p})$ and $\mathbf{b}(\mathbf{p})$ to be constant when the pressure field is calculated, yields a system of linear equations, which gives sufficient accuracy in the flow rates for small timesteps.

2.4 Film Dynamics

In a one-dimensional network, a differential form of Eq. 17 for the water layers may be written as

$$\frac{\partial}{\partial x}\left(g_{\mathrm{w}} l \frac{\partial p_{\mathrm{w}}}{\partial x}\right) = 0. \tag{19}$$

However, this equation assumes that the thickness of the water layer is stationary, which is not the case in our model. The solution to Eq. 19 is the steady solution to the equation of the layer dynamics

$$\frac{\partial}{\partial x}\left(g_{\mathrm{w}} l \frac{\partial p_{\mathrm{w}}}{\partial x}\right) = \frac{\partial A_{\mathrm{w}}}{\partial t}, \tag{20}$$

which takes into account swelling and shrinking of the water layer. However, this equation, together with the corresponding equation for the oil phase, gives a coupled nonlinear diffusion equation. Solving this requires computations that require excessive computational times. We will instead use the steady-state solution given by Eq. 18. As an approximation to the layer dynamics, we then use a linear relation to relax the layer thickness in time. This is analog to the concept used for macroscopic capillary pressure by (Hassanizadeh and Gray 1993), and similar to the procedure implemented by Singh and Mohanty (2003). The relaxation equation for a single node yields

$$\frac{\partial A_{\mathrm{w}}}{\partial t} = K\left(P_{\mathrm{c}} - P_{\mathrm{c}}^{\mathrm{calc}}\right) = K\left(\frac{\gamma}{r_{\mathrm{w}}} - \left(P_{\mathrm{nw}} - p_{\mathrm{w}}\right)\right), \tag{21}$$

where K is a damping coefficient, and $\frac{\gamma}{r_{\mathrm{w}}}$ is the capillary pressure solution obtained from Eq. 18 is denoted $P_{\mathrm{c}}^{\mathrm{calc}} = P_{\mathrm{nw}} - p_{\mathrm{w}}$. Equilibrium is reached when $\frac{\gamma}{r_{\mathrm{w}}} = P_{\mathrm{c}}^{\mathrm{calc}}$. Following the idea of macroscopic equilibrium, K is connected to the mobility of the layer thickness. A very large K means that the thickness of the layers will reestablish to the equilibrium thickness virtually instantaneously. While if K is very small, the layers will swell or shrink very slowly. This means that K is a measure of the rate of change in layer thickness. Singh and Mohanty (2003) used the assumption that the layer conductance is approximately two orders of magnitude smaller than the bulk conductance. To obtain a realistic and consistent value of K, we compare the solution of Eq. 21 with the solution of a nonlinear diffusion process in a single capillary tube of length L, and uniform radius, which represents a simplified version of the network. The tube is illustrated in Fig. 4. One meniscus is present in the tube with a high initial capillary pressure. Then the capillary pressure is decreased, and the meniscus reestablish to a new equilibrium position. Water will start to imbibe into the water layer. By assuming that the pressure in the oil phase is constant, we can combine Eqs. 20, 2, 4, and 5 to the following nonlinear diffusion equation

$$\frac{\partial A_{\mathrm{w}}}{\partial t} = B \frac{\partial}{\partial x}\left(\sqrt{A_{\mathrm{w}}} \frac{\partial A_{\mathrm{w}}}{\partial x}\right), \tag{22}$$

where

$$B = \frac{\gamma}{16\beta\mu_{\mathrm{w}}\sqrt{\frac{1}{4G} - \pi}}. \tag{23}$$

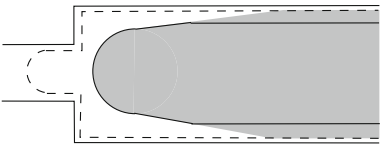

Fig. 4 Illustration of how the water layer (*gray shaded*) is diffusing into a tube according to Eq. 22. The *dashed line* shows the initial position of the meniscus, and the initial layer thickness. The full line shows the final position of the meniscus, and the final layer thickness at $t \to \infty$

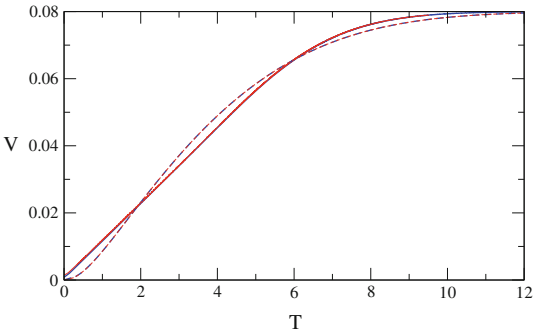

Fig. 5 Scaled volume as a function of scaled time for Eq. 22 (*full red line*), and Eq. 21 (*dashed red line*) for parameters $G = 0.048$, $\mu_w = 1$ mPa s, $\gamma = 30$ mN/m, $L = 4$ mm. Equation 22 (*full blue line*), and Eq. 21 (*dashed blue line*) for parameters $G = 0.04$, $\mu_w = 5$ mPa s, $\gamma = 60$ mN/m, $L = 8$ mm. Note that the curves are collapsed on top of each other

Dong and Chatzis (1995) showed, both theoretically and experimentally, that the imbibed volume V_{imb} at time t yields

$$V_{\text{imb}} \propto \left(\frac{1}{4G} - \pi\right)\left(\frac{\gamma}{\mu_w \beta}\right)^{1/2} t^{1/2}. \tag{24}$$

We now define

$$V = \frac{V_{\text{imb}}}{L\left(\frac{1}{4G} - \pi\right)}, \tag{25}$$

and

$$T = \frac{1}{L}\left(\frac{\gamma}{\mu_w \beta}\right)^{1/2} t^{1/2}. \tag{26}$$

We solve Eq. 22 numerically for the single tube. By plotting V versus T, the curves are collapsing for different values of G, μ, β, γ, and L. This is shown in Fig. 5. In order to collapse Eq. 21 with the same scaled variables V and T, we realize that $V_{\text{imb}} \propto LK\gamma t$. This gives

$$K = \frac{K^*\left(\frac{1}{4G} - \pi\right)}{\mu_w \beta L^2}, \tag{27}$$

where K^* is a constant chosen so that Eq. 21 matches with the diffusion result of Eq. 22, and L is the length of the network. Notice that the initial and final radius of curvature are assumed constant and are included in K^*. We use Eq. 27 also for shrinking of the water layers (drainage), with the same K^* as for swelling. This is partly to ensure a unified model for drainage and imbibition, and because it is reasonable to assume that swelling and shrinking of water layers occur on the same time scale.

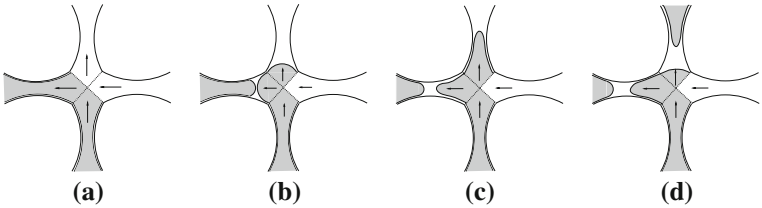

Fig. 6 A mixture of oil (*shaded*) and water (*white*) flow into the node from the right and bottom tubes. The time proceeds from **a** to **d**, and the figures show how the fluid is distributed to the *left* and *top* tube

Combining Eq. 2 with Eq. 21 gives

$$\frac{\partial r_{\mathrm{w}}}{\partial t} = \varrho \left(\frac{\gamma}{r_{\mathrm{w}}^2} - \frac{1}{r_{\mathrm{w}}} (P_{\mathrm{nw}} - p_{\mathrm{w}}) \right), \tag{28}$$

where $\varrho = K/2 \left(\frac{1}{4G} - \pi \right)$. This equation is solved using an implicit finite-difference scheme written as

$$r_{\mathrm{w}}^{n+1} = \varrho \Delta t \left(\frac{\gamma}{(r_{\mathrm{w}}^{n+1})^2} - \frac{1}{r_{\mathrm{w}}^{n+1}} (P_{\mathrm{nw}}^{n+1} - p_{\mathrm{w}}^{n+1}) \right) + r_{\mathrm{w}}^{n}, \tag{29}$$

where $t = n\Delta t$. The nonlinear relation is solved with the Newton–Raphson method. We solve the following system of linear equations once every timestep

$$\mathbf{A} \left(\mathbf{r}_{\mathrm{w}}^{n} \right) \mathbf{p}^{n+1} = \mathbf{b} \left(\mathbf{r}_{\mathrm{w}}^{n} \right), \tag{30}$$

where $\mathbf{r}_{\mathrm{w}}^{n}$ is given by Eq. 29. Equation 30 is solved by a conjugate gradient method. As menisci move through pores and throats, water layers are created. We use the pressure solution of Eq. 18 as an approximation for the capillary pressure close to menisci, and the thickness of a newly created wetting layer is given by

$$r_{\mathrm{w}} = \frac{\gamma}{P_{\mathrm{c}}^{\mathrm{calc}}}. \tag{31}$$

$P_{\mathrm{c}}^{\mathrm{calc}}$ is only calculated in nodes, but wetting layers are created in both nodes and throats. For the throats, r_{w} is given by the entry capillary pressure $P_{\mathrm{c}} = 2\gamma / r_{\mathrm{IJ}}$, which yields $r_{\mathrm{w}} = r_{\mathrm{IJ}}/2$.

2.5 Flow Mechanisms

When menisci positions are updated, we us an effective area of the tubes to calculate the new positions, consistent with Aker et al. (1998). The fluid entering a node each timestep is simply mixed in the node, and distributed to the tubes where it flows out of the node. Excess menisci are coalesced according to rules which are illustrated in Fig. 6. Oil and water is entering the node from the right and bottom tube in Fig. 6a. The fraction of water entering the node will enter the left and top tube, and the fraction of oil will subsequently follow, as we see in Figs. 6b and c. If the size of the oil bubble is more than half of the tube length, and more than 50% water enters the tube, then this bubble is pushed to the other side of the tube. The fraction of water then follows, and finally the fraction of oil enters the tube. This event is illustrated in the upper tube in Fig. 6d. Bubbles of oil in the throat are not accounted for by these rules. The reason is that small bubbles in throats are short-lived and should not be important for the overall properties of the flow.

We choose the timestep so that the meniscus with the highest velocity will move 10% of the length of the tube.

This mixing rules can be justified for high capillary numbers. For low capillary numbers, the approximation becomes less accurate because of cooperative pore filling and additional fluid configurations in pore nodes/bodies that are not accounted for. This limits the applicability range of the model to capillary numbers where both capillary and viscous forced are important.

2.5.1 Snap-off

The most described mechanism behind snap-off is the "Roof snap-off", after the work of Roof (1970) who studied penetration of narrow throats by nonwetting fluid. Due to local capillary pressure gradients caused by the expanding meniscus in a downstream pore, a snap-off will happen if the radius of the pore-body is about twice the radius of the constriction. As the snap-off process repeats itself, some of the bubbles will coalesce into bigger bubbles. Hence, one may argue that snap-off is not important for the displacement in drainage.

Experiments on micromodels by Lenormand et al. (1983), Bernadiner (1998), Tzimas et al. (1997), Kovscek et al. (2007), Li and Wardlaw (1986) show that snap-off in imbibition is an important mechanism for disconnection and trapping of nonwetting fluid at low capillary numbers. The mechanism behind snap-off in imbibition is understood as due to fluctuations in the capillary pressure around a constriction. Snap-off happens when enough fluid has accumulated in the neck of the throat so that the radius of curvature of the water layer reaches a critical value. This is a complicated phenomena, and is linked to the structure of the corners and crevices in the rock. Gauglitz and Radke (1990) examined the dynamics of layer swelling in constricted cylindrical capillaries, and developed a fourth order partial differential equation for the thickness of the layer. They showed that the time for snap-off is dependent on the initial profile of the layer, the film thickness, and the flowrate.

In order to incorporate snap-off in the model, we use a simple criteria for the layer thickness in the throat. At a critical thickness, the oil in the bulk is no longer in contact with the walls, and the oil bubble snaps off. The snap-off results in a collar of water between two bubbles of oil. For a perfectly wetting medium the threshold for snap-off is when r_{w} exceeds the inscribed radius (Ransohoff et al. 1987)

$$r_{\mathrm{w,IJ}} \geq r_{\mathrm{IJ}}. \tag{32}$$

Snap-off is only possible in tubes of type (B). When snap-off happens, the tube is changed into type (D), with a small bubble of water in the throat. This makes it possible for the water to flow from the layer into the bulk. We emphasize that the we use a unified model for drainage and imbibition. Hence, snap-off is possible in drainage, but is a rare event, and is insignificant compared to effect of the mixing rules.

2.6 Boundary Condition

We use non-periodic boundary conditions in all directions. Fluid is injected at the inlet by applying a constant pressure or a constant flowrate. In order to keep a constant flowrate, the pressure in the bulk at the inlet is adjusted using a proportional regulation. To reduce capillary end effects, there will always exist a meniscus in tubes where oil has reached the outlet when a drainage process is performed. Hence, the capillary pressure at the outlet is given

by the radius of curvature of this meniscus. For an imbibition process, the outlet and inlet is interchanged, and an average capillary pressure over the total network is used as capillary pressure at the outlet.

3 Capillary Number

The capillary number Ca is used as a measure of the relative importance of the capillary and viscous forces in immiscible displacement in porous media. It is expressed as

$$\mathrm{Ca} = \frac{\mu v}{\gamma}, \tag{33}$$

where μ is the largest viscosity of the two fluids, and v is the average flow velocity. Since viscous forces are proportional to the length L of the system in the direction of flow, it is more constructive to use a capillary number CA when comparing results for different system lengths. It yields

$$\mathrm{CA} = \frac{4\mathrm{Ca}L}{r_{\mathrm{eff}} \cos\theta}, \tag{34}$$

where r_{eff} is a pore radius characteristic for the system. It is derived for a single cylindrical tube (Dullien 1992). For free spontaneous imbibition, FSI, the viscous force and the capillary force are in balance because the pressure drop across the system is zero. This gives $\mathrm{CA}_{\mathrm{FSI}} = 1$. Imbibition at $\mathrm{CA} < 1$ is referred to as controlled spontaneous imbibition, CSI, and at $\mathrm{CA} > 1$ as forced imbibition, FI. By keeping all parameters in Eq. 34 constant except the flowrate, the value of CA is found by $\mathrm{CA} = q/q_{\mathrm{FSI}}$, where q_{FSI} is the flowrate at free spontaneous imbibition.

4 Results

4.1 The Reconstructed Network

The network is constructed by first generating the pore space using a process based reconstruction. More details can be found in Bakke and Øren (1997). Then the network is extracted by defining pore and throat radii and throat lengths. The simulations are carried out on one realization of size $(4.5 \times 1.5 \times 1.5)$ mm^3 consisting of 767 nodes and 1750 tubes. The porosity is 35%, the permeability is measured to 48 Darcy, and the formation factor is 3. The characteristics of the network are in agreement with sandpacks used by Dong et al. (1998) and Meleán et al. (2003). They performed imbibition experiments for $\mathrm{CA} \approx 0.01$–10 ($\mathrm{Ca} = 10^{-8} - 10^{-5}$) with strongly water-wet conditions at samples about 100 times longer than the network we consider.

The computation time greatly depends on the capillary number. A on this particular network a drainage-imbibition cycle takes about two hours for $\mathrm{CA} = 10$. However, for $\mathrm{CA} = 0.1$ the time increases to a couple of days. Because of the explicit time-stepping and the changing capillary pressure in the tubes the menisci are oscillating back and forth. And as the time step is increased the amount of oscillations also increases. This makes the model inefficient for low capillary numbers. The optimal time step also depends on the capillary number, and to be consistent a time step of 10% of the length of the tubes is chosen.

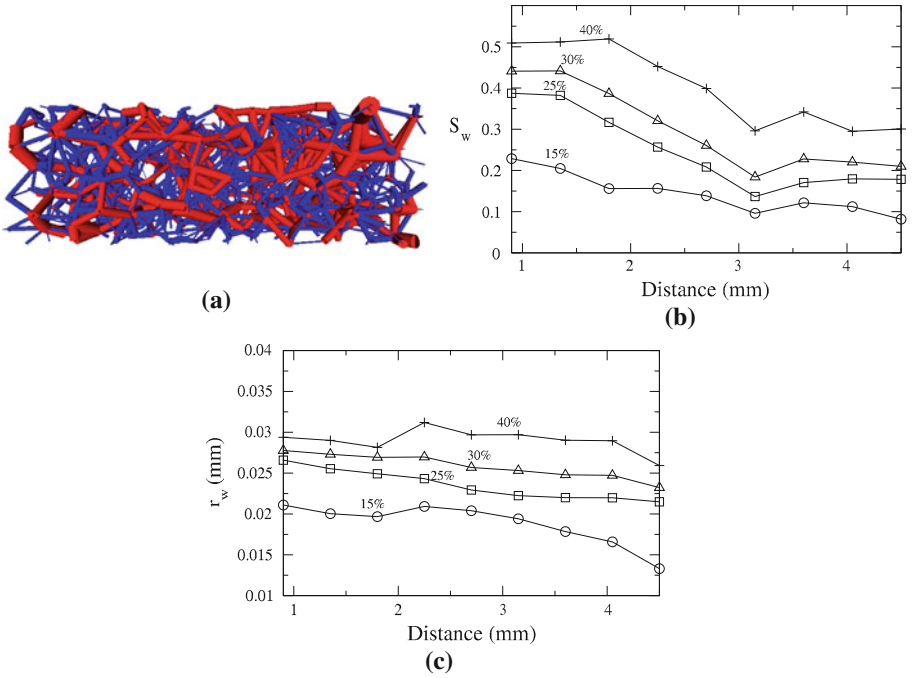

Fig. 7 Controlled spontaneous imbibition at CA $= 0.1$ (Ca $\approx 1.5 \times 10^{-5}$) with $S_{\mathrm{wi}} = 15\%$. Water is injected from the left. **a** Snapshot of oil (*red*) and water (*blue*) in the network for $S_{\mathrm{w}} = 35\%$. **b** Time evolution of the water saturation profile. **c** Time evolution of the radius of curvature profile. The legends show the average network water saturation S_{w}

4.2 Saturation Profiles

We carry out imbibition simulations for capillary numbers ranging from CA $= 0.1$ to CA $=$ 10 with initial water saturation $S_{\mathrm{wi}} = 15\%$. We use equal viscosity $\mu = 1$ mPa s for both phases, and $\gamma = 30$ mN/m. A primary drainage process is performed prior to the imbibition by gradually increasing the applied pressure drop until the desired S_{wi} is reached.

Figure 7a shows a snapshot of the distribution of water (blue color) and oil (red color) during controlled spontaneous imbibition at CA $= 0.1$. Water is injected from the left. There is no distinct front visible, and snap-offs seem to occur randomly across the entire network. This behavior is also visible in Fig. 7b, where the time evolution of the saturation profile is shown. Fig. 7c shows the average radius of curvature r_{w} in cross-sections along the length of the network. The even increase in r_{w} across the network supports the random occurrence of snap-offs.

Figure 8 shows the saturation profiles for free spontaneous imbibition. We measure a capillary number Ca $\approx 1.5 \times 10^{-4}$, which agrees with Ca $\approx 10^{-6}$ obtained by Dong et al. (1998) and Meleán et al. (2003) since they used systems approximately 100 times longer. A water front is visible, where piston-like displacement is dominating and snap-off is suppressed. We also observe a precursor front in the water layers shown in Fig. 8c.

For CA $= 10$ in Fig. 9, the flowrate is so fast that there is insufficient time for the water layers to swell significantly before the water front has passed. This is forced imbibition, and snap-off is totally suppressed.

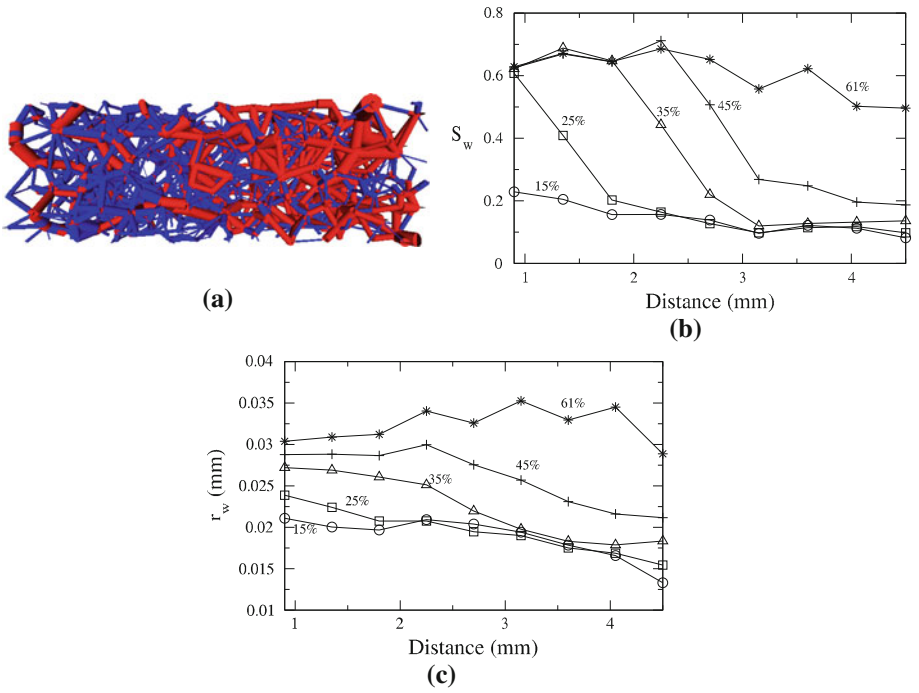

Fig. 8 Free spontaneous imbibition at CA = 1 (Ca $\approx 1.5 \times 10^{-4}$) with $S_{wi} = 15\%$. Water is injected from the left. (**a**) Snapshot of oil (*red*) and water (*blue*) in the network for $S_w = 35\%$. **b** Time evolution of the water saturation profile. **c** Time evolution of the radius of curvature profile. The legends show the average network water saturation S_w

The saturation profiles are in qualitative agreement with experiments of Dong et al. (1998) and Meleán et al. (2003). From CA = 0.1 to CA = 10, there is a transition from uniform change of saturation across the whole network, where snap-off is the dominant displacement mechanism, to a steep front where frontal displacement is dominant. From low to high values of CA, there is also a decrease in the overall thickness of the water layers, due to insufficient time to swell.

Increasing CA is also accompanied with less trapped oil, and a decrease in the residual oil saturation S_{or} (Tzimas et al. 1997; Constantinides and Payatakes 2000). Table 1 gives the S_{or} for the different capillary numbers. For $_{CA} = 0.1$ the obtained $S_{or} = 60\%$ is in agreement with the quasi-static result at $S_{or}(QS) = 62\%$.

4.3 Resistivity Index

Resistivity measurements are used to determine water saturation in hydrocarbon formations. The interpretation of resistivity measurements is usually based on Archie's law, which relates a resistivity index I_R with S_w by

$$I_R(S_w) = \frac{R_{S_w<100\%}}{R_{S_w=100\%}} = S_w^{-n}, \tag{35}$$

where n is the saturation exponent. Experiments by Wei and Lile (1990) and Sweeney and Jennings (1960) have shown that Archie's law is valid only in strongly water-wet rocks. The value of the saturation exponent is close to 2 for such rocks.

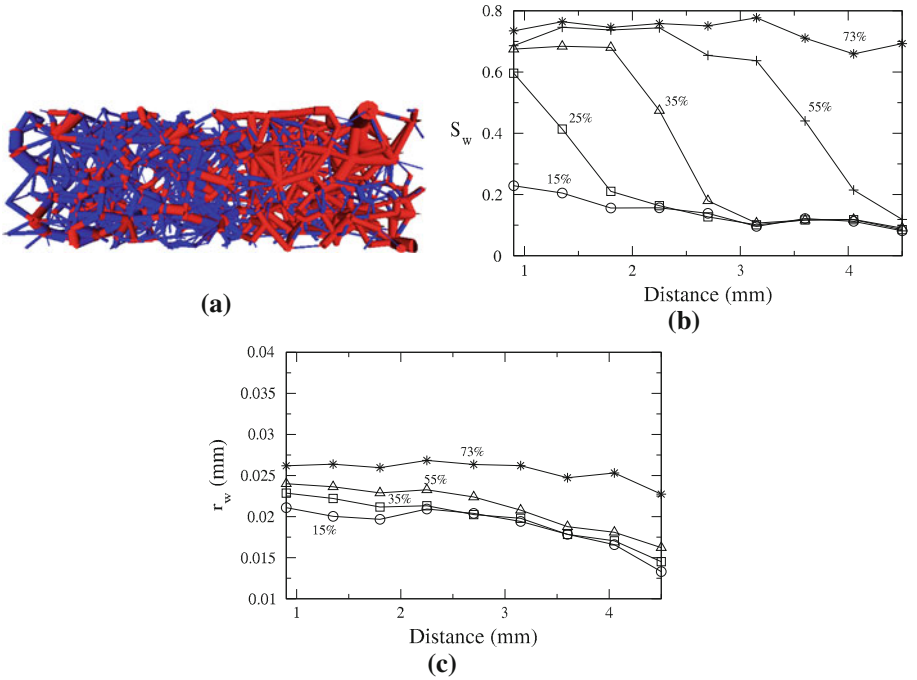

Fig. 9 Forced imbibition at CA = 10 (Ca = 1.5×10^{-3}) with $S_{wi} = 15\%$. Water is injected from the left. **a** Snapshot of oil (*red*) and water (*blue*) in the network for $S_w = 35\%$. **b** Time evolution of the water saturation profile. **c** Time evolution of the radius of curvature profile. The legends show the average network water saturation S_w

Table 1 Residual oil saturation, S_{or}, and the time to reach S_{or}, $t_{S_{or}}$, for different values of *CA*

CA	$S_{or}(\%)$	$t_{S_{or}}$ (s)
0.1	60	8
1	39	2
10	27	0.7

Hysteresis in the resistivity index is often observed (Longeron et al. 1989; Knight 1991). A possible explaination could be that for displacement at low capillary numbers in strongly water-wet rocks, drainage is dominated by piston-like displacement, and imbibition is dominated by snap-off. Snap-off causes trapping of oil clusters, which gives a lower water saturation compared to drainage for a given capillary pressure or resistivity index. Hence, hysteresis is observed.

To calculate the resistivity, we assume that the oil phase is insulating, and that the electrical conductance of a water element is given by

$$g_e = \frac{A\sigma_w}{l}, \tag{36}$$

where A is the cross-sectional area, σ_w is the water resistivity, and l is the length of the element. Water elements within a tube are coupled in series to get an effective conductance for each tube. The resistivity of the network is calculated between the inlet and outlet by applying a voltage drop across the network. We use Kirchhoff's law to evaluate the voltages in the nodes. From the voltages, the total current and resistivity can be found.

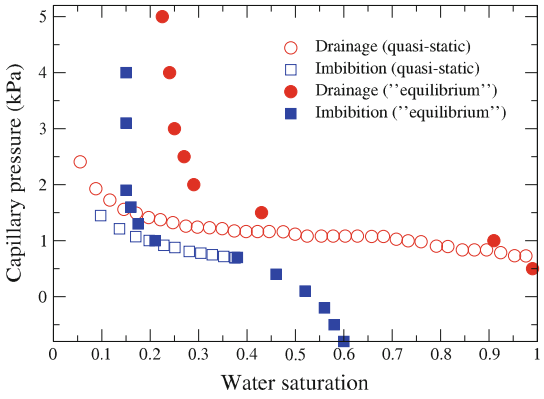

Fig. 10 Comparison of P_c for our model with a quasi-static model (Bakke and Øren 1997). The data points are obtained when the change in the saturation drops below a given threshold

We mimic an experimental drainage–imbibition cycle where the dynamic capillary pressure is given by the applied pressure drop, $\Delta P = P_c$, across the network. Initially the network is completely filled with water. Oil is injected by incrementing ΔP when the change in the saturation drops below a given threshold. This gives a fluctuating capillary number at $\text{Ca} \approx 10^{-5}$ before breakthrough. We name this the "equilibrium" process. Fig. 10 compares "equilibrium" capillary pressure for our model with a quasi-static model. Due to a finite threshold, the dynamic capillary pressure ΔP is larger than P_c of the quasi-static model for drainage (Hassanizadeh and Gray 1993). As S_{wi} is approached, the difference increases due to decreasing hydraulic conductance of the water phase. As the threshold goes to zero, the dynamic capillary pressure will approach the static capillary pressure. The drawback is that the computational cost increases.

The "equilibrium" drainage process is stopped at $S_{wi} = 15\%$, and a subsequent imbibition displacement is performed by decrementing ΔP. Water initially imbibes by CSI at $\text{CA} \approx 0.1$. As the applied pressure continues to drop, FSI and finally, FI is performed. The quasi-static model reaches S_{or} when all the remaining oil is disconnected from the outlet. In the dynamic model, mobilization of disconnected clusters is possible as the applied pressure becomes negative, and $S_{or} = 38\%$ is reached.

Figure 11a shows the profiles of the radius of curvature r_w for the "equilibrium" process. As ΔP increases, and smaller pores are invaded, r_w will decrease. In Fig. 11b a constant flowrate at $\text{Ca} = 5.0 \times 10^{-4}$ is used. ΔP is now initially high, and increasing. This renders r_w initially low and decreasing.

The resistivity index for drainage is shown in Fig. 12a. The saturation exponent is around 1.6 for the "equilibrium" displacement, but we see that the resistivity index tends to curve toward the saturation axis. This kind of "non-Archie" behavior is experimentally observed (Worthington and Pallatt 1992; Moss et al. 1999), and can be explained by the increasing amount of electric current in the water layers as S_w decreases. If water is only residing in water layers, and the connectivity of the layers is preserved, the resistivity index yields $I_R = 1/S_w$. Hence, the saturation exponent approaches 1.

Another observation is that the saturation exponent is increasing with increasing capillary number, in agreement with experiments on core plugs (Jing et al. 1993; Maas et al. 2000) and sandpacks (Aggelopoulos et al. 2005). For drainage at constant flowrate, the resistivity index will approach the "equilibrium" result after breakthrough. Then the displacement will eventually stop, and further increase of the flowrate is needed to mobilize the remaining water.

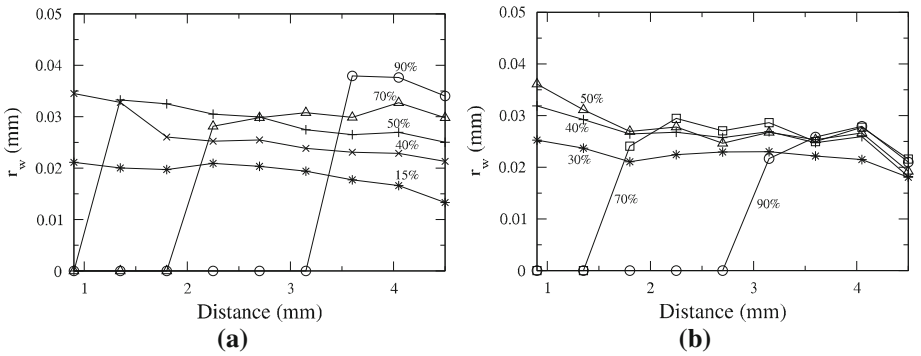

Fig. 11 Time evolution of the profile of r_w in primary drainage. The network is initially filled with water, and the oil is injected from the right. Tubes completely filled with water correspond to $r_w = 0$. The legends show the water saturation S_w. **a** Drainage by the "equilibrium" process (Ca $\approx 10^{-5}$). **b** constant flowrate at Ca $= 5.0 \times 10^{-4}$

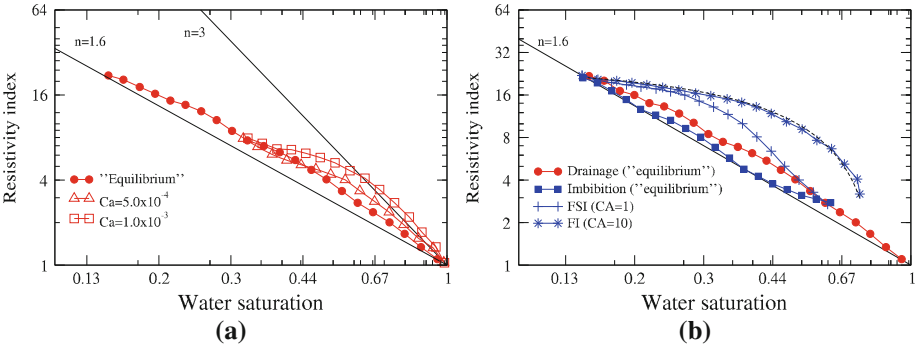

Fig. 12 **a** Log–log plot of the resistivity index for primary drainage at different capillary numbers. **b** Log–log plot of the resistivity index for drainage–imbibition cycles at different capillary numbers. The fitting model of Eq. 37 is indicated by the *dashed line*

The resistivity index for drainage–imbibition cycles is plotted in Fig. 12b. We find a significant hysteresis loop. Some experiments show hysteresis in the resistivity index between drainage and imbibition cycles in water-wet sandstones (Longeron et al. 1989; Knight 1991). However, some authors also report no significant hysteresis (Moss et al. 1999; Han et al. 2007). The shape of the curve for the "equilibrium" imbibition is bending slightly upward, while for FSI and FI the curve is bending downward. This behavior is attributed to the suppressed swelling of the water layers, and the sharp front in imbibition at large capillary numbers. If we assume a constant saturation on each side of the front with S_{or} behind the front, and S_{wi} ahead of the front, then the resistivity index can be expressed by the linear relation

$$I_R(S_w) = I_{S_{or}} + \frac{(1 - S_{or} - S_w)(I_{S_{wi}} - I_{S_{or}})}{1 - S_{or} - S_{wi}}, \tag{37}$$

where $I_{S_{or}}$ and $I_{S_{wi}}$ are the resistivity indices at S_{or} and S_{wi}, respectively. This relation is fitted to the FI result in Fig. 12b.

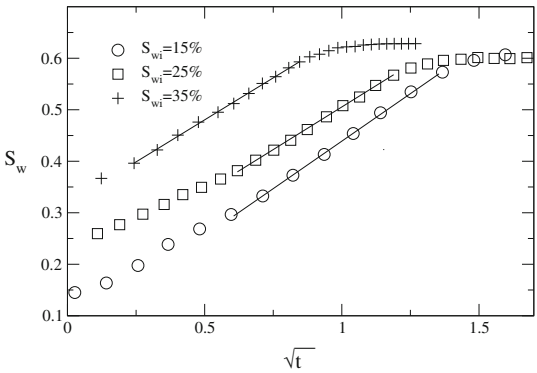

Fig. 13 Imbibition rate for free spontaneous imbibition for different S_{wi}. The *solid lines* indicate the Washburn law

4.4 Free Spontaneous Imbibition Rate

Washburn (1921) provided an early analysis of the free spontaneous imbibition process. He considered water displacing air in a horizontal cylindrical capillary tube. By assuming Poiseuille flow, and that the viscosity of air is negligible, the Washburn law yields

$$x = \sqrt{\frac{\gamma r \cos\theta}{2\mu}}\sqrt{t}, \tag{38}$$

where x is the distance penetrated by the liquid, r is the radius, and μ is the viscosity of the liquid. In the case of viscosity matching, then a linear relation between penetration length and time is found

$$x = \frac{\gamma r \cos\theta}{4\mu l}t, \tag{39}$$

where l is the total length of the tube. These equations explain the basic competition between capillary forces and viscous resistance in a single capillary tube. However, in a porous medium they can be invalidated by many factors. For example, they assume cylindrical tubes with no water layers; furthermore, they assume free supply of water, and thereby predicts that wide tubes are filled faster than narrow tubes. In porous media, however, the narrowest throats are filled first. This may be explained by a limited supply of water to large pores (Chatzis and Dullien 1983; Sorbie et al. 1995). Despite the complicating factors for imbibition in porous media, Washburn behavior is often observed in experiments (Akin et al. 2000; Li et al. 2003; Fisher and Morrow 2005), even when the viscosity of the onwetting phase can not be neglected.

We have conducted free spontaneous imbibition simulation with the dynamic model for different values of S_{wi}. The results are plotted in Fig. 13. It seems that the model follows the Washburn law in an intermediate domain where the front is not influenced by end effects. Note that we have used S_{w} instead of the penetration length x in Eq. 38. This is valid as long as the residual saturation behind the water front is constant with distance from inlet.

5 Conclusion

A fully dynamic model for two-phase immiscible flow in a network has been developed. It can be used as a unified model for drainage, imbibition and steady-state displacement.

In this work, the model has been used on a reconstructed network of a sandpack to reproduce important characteristics at strongly water-wet conditions. For imbibition, we see a sharpening of the water front for increasing capillary numbers, and the saturation profiles are comparable with experimental data from sandpacks for a wide range of capillary numbers. We also simulate drainage–imbibition cycles at different capillary numbers. We find a saturation exponent and hysteresis in the resistivity index that is typically observed in experiments. The imbibition rate for free spontaneous imbibition is found to partially follow the Washburn law.

These preliminary results suggest that the model can mimic experimental setups and reproduce petrophysical parameters at different capillary numbers. In future work, we will focus on measuring electrical resistivity in steady-state displacement.

Acknowledgments This work has been financed by the Norwegian Research Council (NFR) Petromax Program No. 174164/S30, EMGS AS, Statoil AS, and Numerical Rocks AS. Computer time was granted by the Norwegian High Performance Project NOTUR.

References

Aggelopoulos, C., Klepetsanis, P., Theodoropoulou, M., Pomoni, K., Tsakiroglou, C.: Large-scale effects on resistivity index of porous media. J. Contam. Hydrol. **77**(4), 299–323 (2005). doi:10.1016/j.jconhyd.2005.02.002

Aker, E., Måløy, K.J., Hansen, A., Batrouni, G.G.: A two-dimensional network simulator for two-phase flow in porous media. Transp. Porous Media **32**, 163–186 (1998)

Akin, S., Schembre, J.M., Bhat, S.K., Kovscek, A.R.: Spontaneous imbibition characteristics of diatomite. J. Pet. Sci. Eng. **25**(3–4), 149–165 (2000)

Al-Gharbi, M., Blunt, M.: Dynamic network modelling of two-phase drainage in porous media. Phys. Rev. E **71**, 016308 (2005)

Bakke, S., Øren, P.: 3-D pore-scale modelling of sandstones and flow simulations in the pore networks. SPEJ **2**, 136–165 (1997)

Bernadiner, M.: A capillary microstructure of the wetting front. Transp. Porous Media **30**, 251–265 (1998)

Bryant, S., Blunt, M.: Prediction of relative permeability in simple porous media. Phys. Rev. A **46**(4), 2004–2011 (1992). doi:10.1103/PhysRevA.46.2004

Chatzis, I., Dullien, F.: Dynamic Immiscible displacement mechanism in pore doublets: theory versus experiment. J. Colloid Interface Sci. **91**, 199–222 (1983)

Constantinides, G., Payatakes, A.: Effects of precursor wetting films in immiscible displacement through porous media. Transp. Porous Media **38**, 291–317 (2000)

Dahle, H., Celia, M.: A dynamic network model for two-phase immiscible flow. Comput. Geosci. **3**, 1–22 (1999). doi:10.1023/A:1011522808132

Dias, M.M., Payatakes, A.C.: Network models for two-phase flow in porous media part 1: Immiscible microdisplacement of non-wetting fluids. J. Fluid Mech. Digit. Arch. **164**(1), 305–336 (1986a)

Dias, M.M., Payatakes, A.C.: Network models for two-phase flow in porous media part 2: Motion of oil ganglia. J. Fluid Mech. Digit. Arch. **164**(1), 337–358 (1986b)

Dong, M., Chatzis, I.: The imbibition and flow of a wetting liquid along the corners of a square capillary tube. J. Colloid Interface Sci. **172**(2), 278–288 (1995)

Dong, M., Dullien, F., Zhou, J.: Characterization of waterflood saturation profile histories by the 'complete' capillary number. Transp. Porous Media **31**:213–237 (1998)

Dullien, F.: Porous Media: Fluid Transport and Pore Structure. Academic Press, London (1992)

Ferer, M., Bromhal, G.S., Smith, D.H.: Pore-level modeling of immiscible drainage: validation in the invasion percolation and DLA limits. Phys. A **319**, 11–35 (2003). doi:10.1016/S0378-4371(02)01508-X

Fisher, H., Morrow, N.R.: Spontaneous imbibition with matched liquid viscosities. Paper SPE 96812, Dallas, TX (2005)

Gauglitz, P., Radke, C.: The dynamics of liquid film breakup in constricted cylindrical capillaries. J. Colloid Interface Sci. **134**(1), 14–40 (1990)

Han, M., Fleury, M., Levitz, P.: Effect of the pore structure on resistivity index curves. In: International Symposium of the Society of Core Analysts, Calgary, Canada (2007)

Hashemi, M., Sahimi, M., Dabir, B.: Percolation with two invaders and two defenders: volatile clusters, oscillations, and scaling. Phys. Rev. Lett. **80**(15), 3248–3251 (1998). doi:10.1103/PhysRevLett.80.3248
Hassanizadeh, S.M., Gray, W.G.: Thermodynamic basis of capillary pressure in porous media. Water Resour. Res. **29**, 3389–3405 (1993)
Hughes, R.G., Blunt, M.J.: Pore scale modeling of rate effects in imbibition. Trans. Porous Media **40**, 295–322 (2000)
Idowu, N.A., Blunt, M.J.: Pore-scale modelling of rate effects in waterflooding. Transp. Porous Media (2009). doi:10.1007/s11242-009-9468-0
Jing, X., Gillespie, A., Trewin, B.: Resistivity index from non equilibrium measurements using detailed in-situ saturation monitoring. In: SPE Paper 26798, Offshore European Conference, Aberdeen, 7–10 September 1993
Knight, R.: Hysteresis in the electrical resistivity of partially saturated sandstones. Geophysics **56**(12), 2139–2147 (1991)
Knudsen, H., Aker, E., Hansen, A.: Bulk flow regimes and fractional flow in 2D porous media by numerical simulations. Transp. Porous Media **47**, 99–121 (2002)
Kovscek, A., Tang, G.Q., Radke, C.: Verification of roof snap off as a foam-generation mechanism in porous media at steady state. Colloids Surf. A **302**(1–3), 251–260 (2007)
Lenormand, R., Zarcone, C., Sarr, A.: Mechanisms of the displacement of one fluid by another in a network of capillary ducts. J. Fluid Mech. Digit. Arch. **135**(1), 337–353 (1983)
Lenormand, R., Touboul, E., Zarcone, C.: Numerical models and experiments on immiscible displacements in porous media. J. Fluid Mech. Digit. Arch. **189**(1), 165–187 (1988)
Li, Y., Wardlaw, N.C.: The influence of wettability and critical pore-throat size ratio on snap–off. J. Colloid Interface Sci. **109**(2), 461–472 (1986). doi:10.1016/0021-9797(86)90324-3
Li, Y., Morrow, N.R., Ruth, D.: Similarity solution for linear counter-current spontaneous imbibition. J. Pet. Sci. Eng. **39**(3–4), 309–326 (2003). doi:10.1016/S0920-4105(03)00071-8
Longeron, D., Argaud, M., Feraud, J.: Effect of overburden pressure and the nature and microscopic distribution of the fluids on electrical properties of rock samples. J. SPE Form. Eval. **16**(2), 169–179 (1989)
Maas, J., van der Post, N., van der Gyp, K., Coenen, J., Looyestijn, W.: Resistivity index measurements under weak capillary forces. In: Paper SCA2000-18. International SCA Symposium, Abu Dhabi (2000)
Man, H.N., Jing, X.D.: Network modelling of strong and intermediate wettability on electrical resistivity and capillary pressure. Adv. Water Resour. **24**(3–4), 345–363 (2001). doi:10.1016/S0309-1708(00)00061-0
Mason, G., Morrow, N.R.: Capillary behavior of a perfectly wetting liquid in irregular triangular tubes. J. Colloid Interface Sci. **141**(1), 262–274 (1991)
Meleán, Y., Broseta, D., Blossey, R.: Imbibition fronts in porous media: effects of initial wetting fluid saturation and flow rate. J. Pet. Sci. Eng. **39**(3–4), 327–336 (2003)
Mogensen, K., Stenby, E.: A dynamic two-phase pore-scale model of imbibition. Transp. Porous Media **32**, 299–327 (1998)
Mogensen, K., Stenby, E., Banerjee, S., Barker, V.: Comparison of iterative methods for computing the pressure field in a dynamic network model. Transp. Porous Media **37**, 277–301 (1999)
Moss, A.K., Jing, X.D., Archer, J.S.: Laboratory investigation of wettability and hysteresis effects on resistivity index and capillary pressure characteristics. J. Pet. Sci. Eng. **24**(2–4), 231–242 (1999)
Nguyen, V.H., Sheppard, A.P., Knackstedt, M.A., Pinczewski, W.V.: A dynamic network model for imbibition. In: Paper SPE 90365. Proceedings of the SPE International Petroleum Conference, Houston, Texas (2004)
Øren, P.E., Bakke, S.: Reconstruction of berea sandstone and pore-scale modelling of wettability effects. J. Pet. Sci. Eng. **39**(3–4), 177–199 (2003). doi:10.1016/S0920-4105(03)00062-7
Øren, P.E., Bakke, S., Arntzen, O.J.: Extending predictive capabilities to network models. SPEJ **3**, 324–336 (1998)
Patzek, T.W.: Verification of a complete pore network simulator of drainage and imbibition. In: Paper SPE 59312. Improved Oil Recovery Symposium, Tulsa, Oklahoma (2000)
Ransohoff, T.C., Radke, C.J.: Laminar flow of a wetting liquid along the corners of a predominantly gas-occupied noncircular pore. J. Colloid Interface Sci. **121**(2), 392–401 (1988)
Ransohoff, T.C., Gauglitz, P.A., Radke, C.J.: Snap-off of gas bubbles in smoothly constricted noncircular capillaries. AIChE J. **33**, 753 (1987)
Roof, J.: Snap-off of oil droplets in water-wet pores. SPEJ **10**, 85–90 (1970)
Singh, M., Mohanty, K.K.: Dynamic modeling of drainage through three-dimensional porous materials. Chem. Eng. Sci. **58**(1), 1–18 (2003). doi:10.1016/S0009-2509(02)00438-4
Sorbie, K.S., Wu, Y.Z., McDougall, S.R.: The extended washburn equation and its application to the oil/water pore doublet problem. J. Colloid Interface Sci. **174**(2), 289–301 (1995)
Sweeney, S.A., Jennings, H.Y.: Effect of wettability on the electrical resistivity of carbonate rock from a petroleum reservoir. J. Phys. Chem. **64**, 551–553 (1960)

Tzimas, G.C., Matsuura, T., Avraam, D.G., Brugghen, W.V.der , Constantinides, G.N., Payatakes, A.C.: The combined effect of the viscosity ratio and the wettability during forced imbibition through nonplanar porous media. J. Colloid Interface Sci. **189**(1), 27–36 (1997)

Tørå, G., Øren, P.E., Hansen, A.: Dynamic network modeling of resistivity index in a steady-state procedure. In: Paper SPE 135367. Proceedings of the 2010 SPE Annual Technical Conference and Exhibition, Florence, Italy , 19–22 September 2010)

Valvatne, P.H., Blunt, M.J.: Predictive pore-scale modeling of two-phase flow in mixed wet media. Water Resour. Res. **40**, W07406 (2004)

Washburn, E.W.: The dynamics of capillary flow. Phys. Rev. **17**(3), 273–283 (1921)

Wei, J., Lile, O.: Hysteresis of the resistivity index in berea sandstone. Advances in core evaluation I. In: 1st Society of Core Analysts European Core Analysis Symposium (1990)

Wilkinson, D., Willemsen, J.F.: Invasion percolation: a new form of percolation theory. J. Phys. A **16**, 3365–3376 (1983)

Worthington, P., Pallatt, N.: Effect of variable saturation exponent on the evaluation of hydrocarbon saturation. J. SPE Form. Eval. **7**, 331–336 (1992)